

LETTERS

How supercontinents and superoceans affect seafloor roughness

Joanne M. Whittaker¹†, R. Dietmar Müller¹, Walter R. Roest², Paul Wessel³ & Walter H. F. Smith⁴

Seafloor roughness varies considerably across the world's ocean basins and is fundamental to controlling the circulation and mixing of heat in the ocean¹ and dissipating eddy kinetic energy². Models derived from analyses of active mid-ocean ridges suggest that ocean floor roughness depends on seafloor spreading rates³, with rougher basement forming below a half-spreading rate threshold of 30–35 mm yr⁻¹ (refs 4, 5), as well as on the local interaction of mid-ocean ridges with mantle plumes or cold-spots⁶. Here we present a global analysis of marine gravity-derived roughness, sediment thickness, seafloor isochrons and palaeo-spreading rates⁷ of Cretaceous to Cenozoic ridge flanks. Our analysis reveals that, after eliminating effects related to spreading rate and sediment thickness, residual roughness anomalies of 5–20 mGal remain over large swaths of ocean floor. We found that the roughness as a function of palaeo-spreading directions and isochron orientations⁷ indicates that most of the observed excess roughness is not related to spreading obliquity, as this effect is restricted to relatively rare occurrences of very high obliquity angles (>45°). Cretaceous Atlantic ocean floor, formed over mantle previously overlain by the Pangaea supercontinent, displays anomalously low roughness away from mantle plumes and is independent of spreading rates. We attribute this observation to a sub-Pangaeian supercontinental mantle temperature anomaly⁸ leading to slightly thicker than normal Late Jurassic and Cretaceous Atlantic crust⁹, reduced brittle fracturing and smoother basement relief. In contrast, ocean crust formed above Pacific superswells¹⁰, probably reflecting metasomatized lithosphere underlain by mantle at only slightly elevated temperatures¹¹, is not associated with basement roughness anomalies. These results highlight a fundamental difference in the nature of large-scale mantle upwellings below supercontinents and superoceans, and their impact on oceanic crustal accretion.

The relationship between spreading rates and marine basement roughness has predominantly been determined through analysis of near-zero-aged crust on individual profiles across mid-ocean ridges using short-wavelength gravity^{3,4} or bathymetry. This relationship was also found to hold for off-axis oceanic crust at all ages⁵. Short-wavelength roughness in gravity anomalies (~20–160 km wavelength) reflects the roughness of oceanic basement topography⁴. Here we use a 2-min gravity anomaly grid downward continued onto the sea floor based on ref. 12 (Supplementary Fig. 1) to create a root mean square (r.m.s.) marine gravity roughness grid (Fig. 1) using a 100-km-wide Gaussian filter with seamounts and oceanic plateaus masked (Supplementary Fig. 2).

Half-spreading rate and sediment cover (Supplementary Fig. 1) strongly influence basement roughness. These factors are removed to examine the role of other potential factors, such as spreading obliquity, mantle temperature and mantle fertility on basement rough-

ness. Each kilometre of sediment¹³ results in an ~14% decrease in gravity roughness (Fig. 2a). Global half-spreading rates⁷ (1) faster than 35 mm yr⁻¹ result in low gravity roughness (~7 mGal), (2) between 35–15 mm yr⁻¹ result in increasingly rough and variable gravity roughness, and (3) slower than 15 mm yr⁻¹ form high-amplitude gravity roughness (~15 mGal) (Fig. 2b). These results differ from previous findings^{4,5} that suggest gravity roughness continues to increase with decreasing half-spreading rates <15 mm yr⁻¹.

Our results confirm that the relationship between spreading rate and basement roughness is consistent with the 'magma lens' model of mid-ocean ridge formation⁶, where decreasing spreading rates lead to increasing lens depth and decreased melt production, with a relatively rapid transition from a lens to a no-lens situation. Our global results show that roughness is insensitive to half-spreading rate at rates >35 mm yr⁻¹ and <15 mm yr⁻¹, probably representing lens and no-lens situations, respectively, with a transitional stage occurring as half-spreading rates drop from 30–35 to 15 mm yr⁻¹. Crust created at rates <15 mm yr⁻¹ is approximately twice as rough as crust created at rates >35 mm yr⁻¹, consistent with thermo-tectonic cyclicity at slow spreading rates¹⁴.

Residual roughness (Fig. 3) is calculated by removing spreading rate and sediment thickness effects (Fig. 2) from the r.m.s. gravity roughness grid (Fig. 1) to investigate how spreading obliquity and mantle conditions influence basement roughness. Higher angles of spreading obliquity are related to increasing ridge segmentation^{14,15} and seismicity¹⁵, both due to increased brittle fracturing at higher

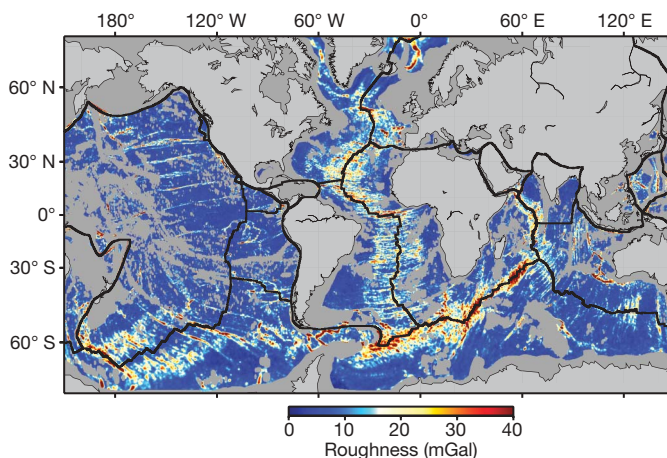


Figure 1 | Downward-continued gravity r.m.s. roughness calculated using a Gaussian filter with a half-width of 50 km. Plate boundaries shown as heavy black lines, landmasses in light grey, and masked continental shelves, seamounts and large igneous provinces in dark grey.

¹Earthbyte Group, School of Geosciences, Building F09, The University of Sydney, Sydney, New South Wales 2006, Australia. ²Ifremer, Centre de Brest, Département des Géosciences Marines, BP 70, 29280 Plouzané, France. ³Department of Geology and Geophysics, SOEST, University of Hawaii at Mānoa, Honolulu, Hawaii 96822, USA. ⁴National Oceanic and Atmospheric Administration, Silver Spring, Maryland 20910, USA. †Present address: GETECH, Kitson House, Elmete Hall, Elmete Lane, Leeds LS8 2LJ, UK.

spreading angles¹⁵. Spreading obliquity has also been found to influence ridge morphology by decreasing effective spreading rates proportionally to $\cos\theta$ (ref. 16), where θ is the angle of obliquity.

To investigate the relationship between spreading obliquity and basement roughness, we create regional 2-min spreading obliquity grids for ten regions (intentionally excluding triple junctions, small/temporary spreading centres, back-arc basins and areas with complex spreading histories; Fig. 3 and Supplementary Figs 5–14) by calculating the difference between the regional plate motion direction and the normal to the regional mid-ocean ridge strike in 5-million-year (5-Myr) stages. Our results show that for spreading obliquities $<45^\circ$, variation of residual roughness with spreading obliquity fits a roughness curve that includes the effective reduction in spreading rate caused by oblique spreading (Fig. 3 inset). However, our analysis also reveals that for obliquities $>45^\circ$, residual roughness increases much more rapidly, indicating that an additional mechanism, probably brittle fracturing, causes increased roughness at high spreading obliquities.

Analysis of residual roughness is carried out for each selected spreading system (Fig. 4) based on spreading rate, sediment thickness and r.m.s. gravity roughness (see Supplementary Fig. 15 for an example of how the sediment thickness–roughness relationship improves the predicted roughness for individual flanks of the South Atlantic spreading system). Only in the North and South Pacific is basement roughness accurately predicted using spreading rate and sediment thickness. With the additional removal of roughness related to spreading obliquity, the roughness of the Southeast Indian ridge flanks is well predicted, while the misfit for the South American–Antarctic ridge is reduced. However, spreading rate, sediment thickness and spreading obliquity do not accurately predict basement roughness for the remaining regions that exhibit long-term deviations of 5–20 mGal over periods >40 Myr and in many cases >60 Myr (Fig. 4).

Relatively smooth basement is predicted for the Australian–Antarctic discordance (AAD) based on half-spreading rates of 35–40 mm yr⁻¹ since ~ 40 Myr ago. However, the AAD exhibits basement

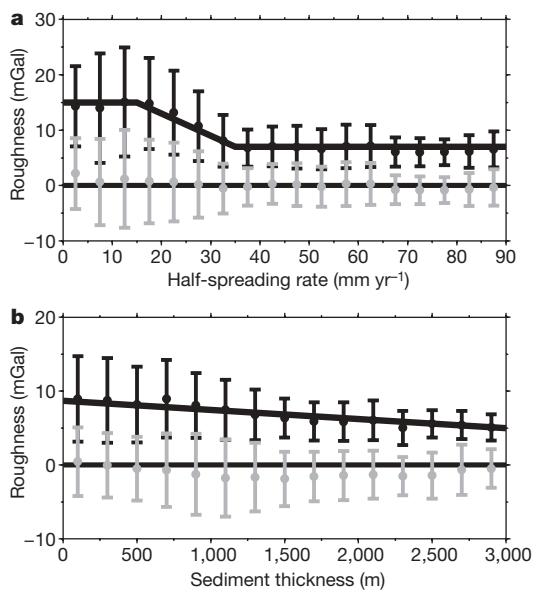


Figure 2 | Gravity roughness as a function of half-spreading rates and sediment thickness. Median roughness and its median absolute deviation were calculated in bins sized 5 mm yr⁻¹ for half-spreading rates (a) and 200 m for sediment thickness (b; filled black circles). Dark grey lines on each graph shows line of best fit, which is used to remove the effects of spreading rate and sediment thickness from gravity roughness. Light grey filled circles show variation of residual gravity roughness (see Fig. 3), with spreading rate (a) and sediment thickness (b). Error bars show \pm median absolute deviation.

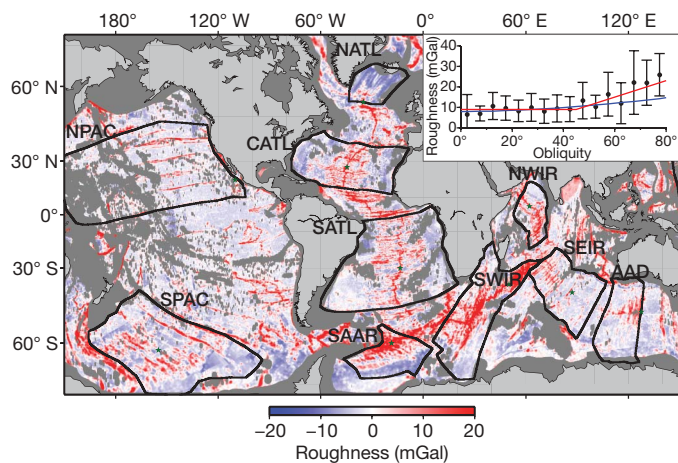


Figure 3 | Residual roughness, after removing effects of spreading rate and sediment thickness from the r.m.s. roughness grid. Main panel: black lines, individual spreading systems; green stars, locations where spreading direction through time was calculated for each region. NPAC, North Pacific; SPAC, South Pacific; NATL, North Atlantic; CATL, Central Atlantic; SATL, South Atlantic; SAAR, South American–Antarctic ridge; SWIR, Southwest Indian ridge; NWIR, Northwest Indian ridge; SEIR, Southeast Indian ridge; AAD, Australian–Antarctic discordance. Inset, relationship between roughness and spreading obliquity. Error bars, median absolute deviation; red line, two-stage line of best fit; blue line, basement roughness expected due to the influence of spreading obliquity on spreading rates assuming roughness equals 8 mGal at 0°.

up to 8 mGal rougher than predicted (Fig. 4). Crustal thickness in the AAD is 2–4 km thinner than adjacent crust, implying a 150 °C decrease in mantle temperature¹⁷. Also, the AAD is located at the site of a palaeosubduction zone, with current lavas probably sourced from depleted magmas derived from subducted oceanic crust¹⁸. Mantle fertility additionally affects the bulk extent of melting^{19,20}, with depleted mantle producing lower melt volumes²¹ and thus rougher basement. Both cool mantle temperatures and low mantle fertility have resulted in rough basement in the AAD despite relatively fast spreading rates over the past 15 Myr (ref. 22).

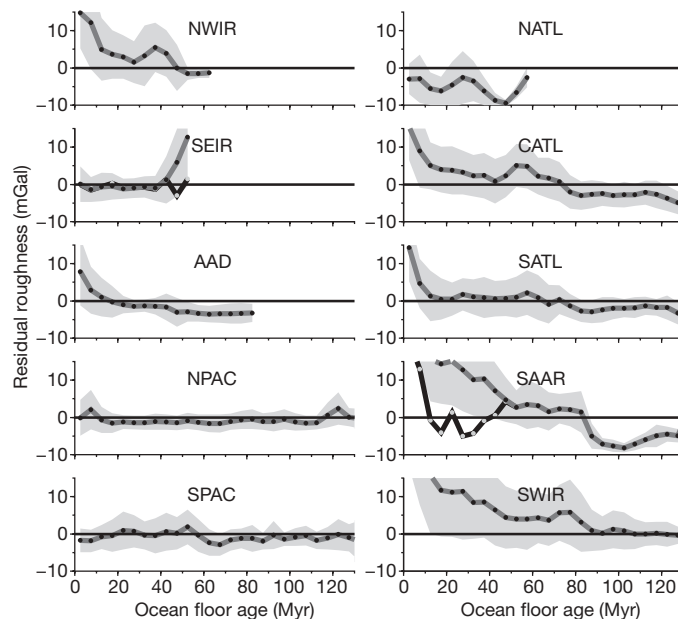


Figure 4 | Variation of residual roughness in 5-Myr stages for ten selected regions. Grey line with black dots, residual roughness for regions shown on plots. Grey envelope, \pm median absolute deviation. Black line with grey dots, residual roughness with roughness attributable to spreading obliquity removed using the relationship shown by the red line in Fig. 3 inset.

We suggest that remaining long-term residual roughness variations, after the removal of roughness caused by variations in spreading rate and sediment cover, are attributable to the temperature and fertility conditions of the underlying mantle. Cretaceous (80–130 Myr old) oceanic crust is smoother than expected, expressed by negative residual roughness (-3 to -9 mGal), mainly in the Central and South Atlantic regions. These regions formed at slow half-spreading rates (<30 mm yr $^{-1}$) during the initial stages of continental dispersal and are associated with pre-breakup magmatism that has been suggested to be unrelated to plume activity^{8,23}. Smoother than expected crust occurs over a vast spatial and temporal domain (over 9,000 km in length and over ~ 50 Myr), supporting a non-plume-related formation mechanism.

Previously, anomalously thick Cretaceous crust on the North American side of the Atlantic has been attributed to a mantle plume influence⁹. However, our analysis shows that both sides of the Atlantic have Cretaceous crust that is smoother than expected (Supplementary Fig. 16), over an area too vast to be related to hotspot related anomalous mantle. We propose that the majority of preserved Cretaceous oceanic crust accreted from anomalously hot supercontinent mantle following Pangaea break-up. Continental aggregation may cause an enlargement of mantle convection wavelengths leading to mantle temperatures up to 100 °C hotter than normal beneath supercontinents⁸. This mantle thermal anomaly is dissipated through seafloor spreading following supercontinent break-up. The anomalously hot mantle would lead to thicker crust and reduced brittle fracturing even under slow spreading conditions.

The North Pacific is the only region with substantial volumes of preserved 80–130-Myr-old crust that did not form through supercontinent break-up. Here spreading rate and sediment thickness accurately predict basement roughness despite the influence of the Cretaceous North Pacific Darwin rise superswell (~ 120 – 85 Myr ago), which may be expected to lead to anomalously smooth basement due to increased heat flow and partial melting¹⁰. At present the South Pacific is underlain by the similar South Pacific superswell¹⁰, which also does not lead to smoother (or rougher) than expected basement. Our observations suggest that Pacific superswells, although causing widespread shallowing of the sea floor¹⁰ and widespread, small-scale alkaline volcanism¹¹, do not strongly influence accretionary processes at mid-ocean ridges. This may reflect metasomatized Pacific superswell lithosphere underlain by mantle at only slightly elevated temperatures, having a negligible effect on mid-ocean ridge accretionary processes. South Pacific superswell initiation has been suggested to reflect a slab-avalanche event leading to slab detachment at the mantle transition zone¹¹. However, a recent plate kinematic model²⁴ leads to the suggestion that the South Pacific superswell was triggered by the well-mapped Eocene plate reorganization, associated with Izanagi-Pacific ridge subduction and subduction initiation along Tonga-Kermadec and the Marianas. The descending slabs of these newly formed subduction zones probably progressively impeded the southwest flow of sub-Pacific mantle²⁴, known to halt at 47 Myr ago²⁵ and triggering an upper mantle return flow ultimately causing anomalously shallow regional sea floor. Our hypothesis provides a mechanism that explains the ongoing nature of the South Pacific superswell, including a lack of influence on seafloor roughness, as opposed to a temporal, catastrophic mantle avalanche mechanism.

Our results provide observational evidence for a fundamental difference between the long-term mantle evolution below supercontinents and superoceans. Supercontinent assembly may lead to a 100 °C warming of sub-continental mantle, whereas associated sub-oceanic mantle stays relatively constant in temperature⁸. During supercontinent dispersal, newly formed spreading ridges initially sample anomalously hot mantle, whereas normal ocean crust in the antipodal superocean is not similarly affected. Considering that continental break-up occurred in the central North Atlantic at about 175 Myr ago²⁶, and that we observe anomalously smooth regional

oceanic basement roughness until 80 Myr ago, it takes nearly 100 Myr for supercontinental mantle warming to dissipate.

Many of the spreading systems analysed here experienced a shift from smoother to rougher than expected basement at ~ 70 Myr ago (central and southern Atlantic systems) and ~ 50 Myr ago (western Indian systems). This may partly reflect the gradual dissipation of a supercontinent-related thermal anomaly, but this alone would not account for a shift to a positive roughness anomaly. Upper mantle depletion is known to reduce melt volumes²¹. The western Indian and central and southern Atlantic mid-ocean ridges are relatively distal to large mantle plumes, resulting in poor upper mantle replenishment because of their dependence on slow, localized mantle upwellings²⁷. An unusual geochemical signature indicates that depleted rather than cold mantle is at least partly responsible for anomalously rough basement at the Southwest Indian ridge²¹. We interpret anomalously rough basement formed during the Cenozoic in the Atlantic and western Indian oceans as reflecting a gradual migration of mid-ocean ridges away from major mantle upwellings²⁸, depriving spreading centres of asthenospheric replenishment.

Contrary to previous studies, our results demonstrate that mantle temperature/fertility and spreading obliquity can dominate spreading rate effects on oceanic basement roughness. As ocean mixing is strongly influenced by seafloor topography, realistic palaeoceanographic simulations depend on reconstructed ocean basin topography, including palaeo-gateways underlain by now subducted crust. Our model provides a predictive framework for reconstructing more realistic maps of ancient ocean basins—a necessary prerequisite for understanding ocean circulation and mixing through time.

METHODS SUMMARY

We high-pass filter the downward-continued gravity grid using a Gaussian filter of 100-km width, then calculate a Gaussian-weighted r.m.s. for these residuals with the same filter width (Fig. 1). Short-wavelength roughness in gravity anomalies (~ 20 – 160 -km wavelength) reflects the roughness of oceanic basement topography⁵. By computing a roughness grid based on a filter width of 160 km following ref. 5 we find that many basement tectonic features are not well resolved (Supplementary Fig. 4). This reflects the fact that the vast majority of structural features of the sea floor such as abyssal hills, fracture zone troughs and ridges have wavelengths significantly smaller than 160 km. We select a 100-km filter width to better resolve spatial variations in seafloor roughness on relatively small scales (Supplementary Fig. 4). The spreading rate dependence of roughness is analysed here in 5-Myr intervals. Intraplate seamount trails and large igneous provinces, rough features formed by non-accretionary processes, are masked from the basement roughness grid using a mask based on a seamount catalogue²⁸ and outlines of oceanic plateaux²⁹. The mapped seamount radii are multiplied by a factor of 2.5 to mask out flexural effects from seamount emplacement. Without this masking the roughness becomes biased by intraplate volcanism unrelated to mid-ocean ridge processes (Supplementary Fig. 2).

Full Methods and any associated references are available in the online version of the paper at www.nature.com/nature.

Received 9 July; accepted 17 October 2008.

- Polzin, K. L., Toole, J. M., Ledwell, J. R. & Schmitt, R. W. Spatial variability of turbulent mixing in the abyssal ocean. *Science* **276**, 93–96 (1997).
- Gille, S. T., Yale, M. M. & Sandwell, D. T. Global correlation of mesoscale ocean variability with seafloor roughness from satellite altimetry. *Geophys. Res. Lett.* **27**, 1251–1254 (2000).
- Malinverno, A. Inverse square-root dependence of mid-ocean-ridge flank roughness on spreading rate. *Nature* **352**, 58–60 (1991).
- Small, C. & Sandwell, D. T. An abrupt change in ridge-axis gravity with spreading rate. *J. Geophys. Res.* **94** (B12), 17383–17392 (1989).
- Smith, W. H. F. Seafloor tectonic fabric from satellite altimetry. *Annu. Rev. Earth Planet. Sci.* **26**, 697–747 (1998).
- Chen, Y. J. in *Ophiolites and Oceanic Crust: New Insights from Field Studies and the Ocean Drilling Program* (eds Dilek, Y. et al.) 161–179 (Special Paper 349, Geological Society of America, 2000).
- Müller, R. D., Sdrolias, M., Gaina, C. & Roest, W. R. Age, spreading rates and spreading asymmetry of the world's ocean crust. *Geochem. Geophys. Geosyst.* **9**, doi:10.1029/2007GC001743 (2008).
- Coltice, N., Phillips, B. R., Bertrand, H., Ricard, Y. & Rey, P. Global warming of the mantle at the origin of flood basalts over supercontinents. *Geology* **35**, 391–394 (2007).

9. Minshull, T. A. On the roughness of Mesozoic oceanic crust in the western North Atlantic. *Geophys. J. Int.* **136**, 286–290 (1999).
10. McNutt, M. K. Superswells. *Rev. Geophys.* **36**, 211–244 (1998).
11. Finn, C. A., Müller, R. D. & Panter, K. S. A Cenozoic diffuse alkaline magmatic province (DAMP) in the southwest Pacific without rift or plume origin. *Geochem. Geophys. Geosyst.* **6**, Q02005. doi:10.1029/2004GC000723 (2005).
12. Sandwell, D. T. & Smith, W. H. F. Retracking ERS-1 altimeter waveforms for optimal gravity field recovery. *Geophys. J. Int.* **163**, 79–89 (2005).
13. Divins, D. L. *Total Sediment Thickness of the World's Oceans and Marginal Seas* (National Geophysical Data Center, 2004); available at (<http://www.ngdc.noaa.gov/mgg/sedthick/sedthick.html>).
14. Abelson, M. & Agnon, A. Mechanics of oblique spreading and ridge segmentation. *Earth Planet. Sci. Lett.* **148**, 405–421 (1997).
15. de Alteriis, G., Gilg-Capar, L. & Olivet, J. L. Matching satellite-derived gravity signatures and seismicity patterns along mid-ocean ridges. *Terra Nova* **10**, 177–182 (1998).
16. Montesi, L. G. J. & Behn, M. D. Mantle flow and melting underneath oblique and ultraslow mid-ocean ridges. *Geophys. Res. Lett.* **34**, doi:10.1029/2007GL031067 (2007).
17. West, B. P., Sempere, J. C., Pyle, D. G., Phipps Morgan, J. & Christie, D. M. Evidence for variable upper mantle temperature and crustal thickness in and near the Australian-Antarctic Discordance. *Earth Planet. Sci. Lett.* **128**, 135–153 (1994).
18. Ritzwoller, M. H., Shapiro, N. M. & Leahy, G. M. A resolved mantle anomaly as the cause of the Australian-Antarctic Discordance. *J. Geophys. Res.* **108** (B12), 2559–2575 (2003).
19. Langmuir, C. H., Klein, E. M. & Plank, T. in *Mantle Flow and Melt Generation at Mid-Ocean Ridges* (eds Phipps Morgan, J., Blackman, D. K. & Sinton, J. M.) 183–280 (Geophysical Monograph 71, American Geophysical Union, 1992).
20. Klein, E. M. & Langmuir, C. H. Global correlations of ocean ridge basalt chemistry with axial depth and crustal thickness. *J. Geophys. Res.* **92** (B8), 8089–8115 (1987).
21. Meyzen, C. M., Toplis, M. J., Humler, E., Ludden, J. N. & Mevel, C. A discontinuity in mantle composition beneath the southwest Indian ridge. *Nature* **42**, 731–733 (2003).
22. Marks, K. M., Stock, J. M. & Quinn, K. J. Evolution of the Australian-Antarctic discordance since Miocene time. *J. Geophys. Res.* **104** (B3), 4967–4981 (1999).
23. McHone, J. Non-plume magmatism and rifting during the opening of the central Atlantic Ocean. *Tectonophysics* **316**, 287–296 (2000).
24. Whittaker, J. *et al.* Major Australian-Antarctic plate reorganization at Hawaiian-Emperor bend time. *Science* **318**, 83–86 (2007).
25. Tarduno, J. A. *et al.* The Emperor Seamounts: Southward motion of the Hawaiian hotspot plume in Earth's mantle. *Science* **301**, 1064–1069 (2003).
26. Klitgord, K. & Schouten, H. in *The Western North Atlantic Region, DNAG Vol. M* (eds Vogt, P. R. & Tucholke, B. E.) 351–378 (Geological Society of America, 1986).
27. Meyzen, C. M. *et al.* Isotopic portrayal of the Earth's upper mantle flow field. *Nature* **447**, 1069–1074 (2007).
28. Wessel, P. Global distribution of seamounts inferred from gridded Geosat/ERS-1 altimetry. *J. Geophys. Res.* **106** (B9), 19431–19441 (2001).
29. Coffin, M. F. & Eldholm, O. Large igneous provinces: Crustal structure, dimensions, and external consequences. *Rev. Geophys.* **32**, 1–36 (1994).

Supplementary Information is linked to the online version of the paper at www.nature.com/nature.

Author Contributions W.H.F.S. contributed to gravity field modelling and the downward continuation. P.W. created the seamount/LIP mask and performed major extensions to *grdfilter* to compute r.m.s. roughness on a Mercator-projected grid. W.R.R. was an initiator of the project who initially explored the effect of both rate and spreading obliquity on roughness. R.D.M. was an initiator of this project, and PhD supervisor of J.M.W., who conceived the idea that supercontinent and superocean effects may drive large-scale roughness anomalies. He and W.R.R. explored workflows to analyse the dependence of seafloor roughness on factors other than spreading rate, and created initial roughness grids, which were improved by the approach implemented by J.M.W. J.M.W. executed the entire project, and combined the various existing ideas and program fragments together into a coherent workflow that allowed systematic testing of ideas and quantification of the supercontinent/superocean hypothesis.

Author Information Reprints and permissions information is available at www.nature.com/reprints. Correspondence and requests for materials should be addressed to J.M.W. (jw@getech.com).

METHODS

We use a global grid of gravity anomalies based on satellite altimetry, downward continued and draped onto the lowpass of the topo_8.2.img grid of the sea floor^{4,30}, using the filters described in ref. 31 to create a global grid of oceanic basement roughness. Our roughness filter is a variable-width Gaussian filter adjusted to the local scale of the Mercator-projected data, whose half-power point wavelength is 50 km, reflecting gravity anomalies due to uncompensated basement topography, implemented in the Generic Mapping Tools program `grdfilter`. This weighted-average filter is applied to individual points to compute r.m.s. marine gravity roughness. To separate the effects of processes related to seafloor spreading, we mask roughness attributable to intraplate seamount trails and large igneous provinces using masks from refs 28 and 29. The mapped seamount radii are multiplied by a factor of 2.5 to mask out flexural effects from seamount emplacement.

Analysis of the relationship between gravity-derived roughness and spreading rate and sediment thickness were conducted using global grids of sediment thickness³, half-spreading rates⁷ and oceanic basement roughness. All grids had the same mask of continental crust, seamounts²⁸ and LIPS²⁹ applied.

The residual roughness grid was calculated by removing the effects of spreading rate and sediment thickness from the gravity-derived roughness grid. The linear relationships between spreading rate and sediment thickness and gravity-derived roughness (Fig. 2) were used to create a predicted roughness grid, which was then subtracted from the r.m.s. gravity-derived roughness grid.

Ten regions were selected to investigate the relationship between roughness and spreading obliquity. Regions were selected to intentionally exclude triple-junctions, small/temporary spreading centres, back-arc basins and areas with complex spreading histories. The 2-min obliquity grids were computed by calculating the difference between the regional plate motion direction (derived from the plate tectonic model of ref. 7) and the normal to the regional strike of the reconstructed mid-ocean ridge based on ref. 7, in 5-Myr stages. All relevant digital grids can be downloaded from www.earthbyte.org.

30. Sandwell, D. T. & Smith, W. H. F. Marine gravity anomaly from Geosat and ERS-1 satellite altimetry. *J. Geophys. Res.* **102** (B5), 10039–10054 (1997).

31. Smith, W. H. F. & Sandwell, D. T. Bathymetric prediction from dense satellite altimetry and sparse shipboard bathymetry. *J. Geophys. Res.* **99** (B11), 21803–21824 (1994).